Distortion modes and related ferroic properties of the stuffed tridymite-type compounds $SrAl_2O_4$ and $BaAl_2O_4$

J. M. Perez-Mato,[1] R. L. Withers,[2] A.-K. Larsson,[2] D. Orobengoa,[1] and Y. Liu[2]
[1]*Departamento de Fisica de la Materia Condensada, Facultad de Ciencia y Tecnologia, Universidad del Pais Vasco (UPV-EHU), Apdo. 644, 48080 Bilbao, Spain*
[2]*Research School of Chemistry, Australian National University, Canberra, A.C.T, 0200, Australia*
(Received 3 November 2008; published 27 February 2009)

The structural and associated ferroic properties of the stuffed tridymite-type compounds $BaAl_2O_4$ and $SrAl_2O_4$ have been investigated by means of *ab initio* calculations. Structures and energy landscapes have been analyzed in terms of symmetry-adapted distortion modes. Despite their rather different room-temperature symmetries, a triply-degenerate unstable antiferrodistortive rigid unit mode (RUM) of the Al_2O_4 tetrahedral framework is shown to be the dominant instability for both compounds. An orthorhombic configuration resulting from a single wave (1**q**) distortion mode competes with a hexagonal configuration resulting from three superposed such waves (3**q**). The very small energy difference between these two configurations in the case of $BaAl_2O_4$ would explain the recent electron microscope observation of orthorhombic symmetry on the nanoscale. A second unstable mode of polar character (also a RUM for the tetrahedral framework) is also present. While this second instability is too weak to condense in $BaAl_2O_4$, in the case of $SrAl_2O_4$ it is fundamental to make the 1**q** configuration prevail. The condensation of this additional instability is the cause of the symmetry reduction in $SrAl_2O_4$ to monoclinic. In contrast with previous literature, $SrAl_2O_4$ is a proper ferroelectric and a pseudoproper ferroelastic, with an uncommon bilinear coupling between its spontaneous polarization and shear monoclinic strain. One expects direct switching of spontaneous polarization through a shear stress, and conversely switching of the ferroelastic spontaneous shear strain through an electric field. This property must be related to the elasticoluminescent and electroluminiscent properties reported in Eu-doped $SrAl_2O_4$. The calculated energy maps have been systematically compared with variations in the so-called *global instability index*, introduced within the empirical bond valence model. The similarity of the variation in both quantities (for the most unstable distortion modes) reported in other systems is also observed here.

DOI: 10.1103/PhysRevB.79.064111 PACS number(s): 77.80.−e, 61.50.Ks, 77.84.−s, 64.70.K−

I. INTRODUCTION

There has long been interest in the crystal structures and polymorphic phase transformation behavior of $BaAl_2O_4$ and $SrAl_2O_4$, both as a result of the inherent displacive flexibility of their stuffed tridymite-type tetrahedral framework structures[1–6] and because of their ferroic properties[7–10] and potential use as host materials for long afterglow luminescence.[11,12] Intense additional interest in $SrAl_2O_4$ has recently been generated by the discovery that $SrAl_2O_4:Eu^{2+}$ (SAO-E) exhibits a visible green wide band emission induced by, and directly proportional to, weak applied elastic stress, a phenomenon known as elasticoluminescence (elastico-L).[13–16] Strong elastico-L materials such as SAO-E show great promise for use in stress sensing devices.[13–16]

The hexagonal $P6_322$ aristotype, and highest-temperature (HT) parent structure, of these compounds is shown in projection along the mutually orthogonal $[001]_p$, $[100]_p$, and $[120]_p$ axes in Figs. 1(a)–1(c) (subscript p for parent), following Refs. 5 and 9. The constituent AlO_4 tetrahedra are significantly rotated around the c_p axis relative to the ideal $P6_3/mmc$ tridymite tetrahedral framework substructure [see Fig. 1(a)], thereby lowering the parent space-group symmetry to $P6_322$. Note that $P6_322$ space-group symmetry does not allow the apical O(1) oxygen ion [see Fig. 1(b)] linking neighboring AlO_4 tetrahedra along c to displace off the local threefold axis in an ordered fashion, giving rise to numerous energetically unfavorable 180° Al-O-Al angles.[17] It is therefore not surprising that a parent structure of this type is not truly stable either at room temperature or, indeed, even at high temperature. Thus a recent $P6_322$ room-temperature structure refinement of $(Ba_{0.6}Sr_{0.4})Al_2O_4$ (Ref. 18) reported a threefold-disordered off-center O(1) oxygen ion, while a recent high-temperature $P6_322$ structure refinement of $SrAl_2O_4$ (Ref. 5) again found a split O(1) oxygen ion and anisotropic displacement parameters, strongly suggestive of coupled tetrahedral rotation about basal plane axes.

On cooling from high temperature to below ~450 K in the case of $BaAl_2O_4$, additional $\mathbf{G} \pm \frac{1}{2}\langle 010\rangle_p^*$ satellite reflections (we label parent Bragg reflections as **G**) appear, giving rise to what appears to be a metrically hexagonal triple-**q** superstructure phase ($\mathbf{a}=2\mathbf{a}_p$, $\mathbf{b}=2\mathbf{b}_p$, $\mathbf{c}=\mathbf{c}_p$) of space-group symmetry $P6_3$.[6,19] A refined crystal structure of this type[6,19] allows $\frac{3}{4}$ of the AlO_4 tetrahedra to be significantly tilted around a basal plane axis. For the remaining $\frac{1}{4}$ of the AlO_4 tetrahedra, however, the local Al-O-Al angle remains at 180°. This $P6_3$ $2a_p \times 2b_p \times c_p$ structure[19] has long been accepted as the room-temperature crystal structure of $BaAl_2O_4$. Very recently, however, fast Fourier transformation of $[001]_p$ lattice images from small localized real-space regions (~10 nm in size) have been used to show that this hexagonal crystal structure for $BaAl_2O_4$ is not correct on the nanoscale and that the true local symmetry is either orthorhombic or monoclinic.[6]

A ferrielectric mechanism was first proposed[8] to explain the room-temperature ferroelectric properties of

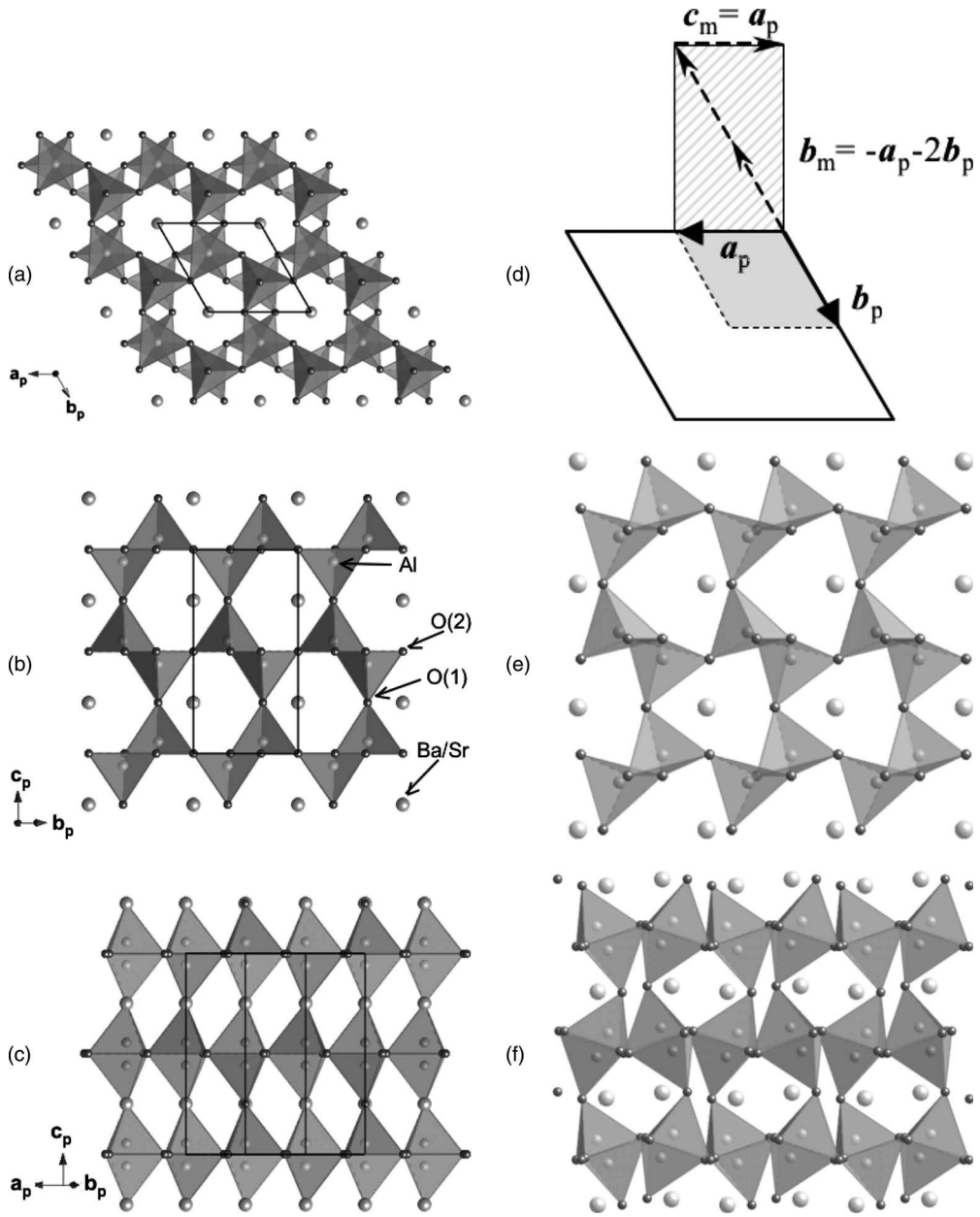

FIG. 1. The hexagonal $P6_322$ aristotype and highest-temperature parent structure of both $SrAl_2O_4$ and $BaAl_2O_4$ are shown in projection along the mutually orthogonal $[001]_p$, $[100]_p$, and $[120]_p$ axes in Figs. 1(a)–1(c) (subscript p for parent). (d) a graphical presentation of the various cell settings and unit cells for the various phases of $SrAl_2O_4$ and $BaAl_2O_4$ described in the text. (e) a $[100]_p$ projection of the parent structure plus the Γ_6 distortion mode of $SrAl_2O_4$ for comparison with the equivalent projection of the parent $P6_322$ structure shown in (b). (e) a $[120]_p$ projection of the parent structure plus the M_2-1**q** distortion mode of $SrAl_2O_4$ for comparison with the equivalent projection of the parent $P6_322$ structure shown in (c).

$BaAl_2O_4$,[7,8,10] assuming the above-mentioned $P6_3$ $2a_p \times 2b_p \times c_p$ structure. More recently, a first-principles study[9] classified the system as an improper ferroelectric (no intrinsic polar instability), again assuming the $P6_3$ $2a_p \times 2b_p \times c_p$ crystal structure. The fact that the local symmetry of this phase is given by a rather different symmetry than $P6_3$, however, demands a reconsideration of our understanding of the ferroelectric features of this compound.

In the case of $SrAl_2O_4$, a recent detailed *in situ* powder-diffraction study[5] has shown two structural phase transitions on cooling. A first transition occurs at ~1130 K to an intermediate $P6_3$ phase ($\mathbf{a}' = -\mathbf{a}_p - 2\mathbf{b}_p$, $\mathbf{b}' = 2\mathbf{a}_p + \mathbf{b}_p$, $\mathbf{c}' = \mathbf{c}_p$) and then a lower temperature phase transition takes place at ~950 K into the final monoclinic $P2_1$ phase ($\mathbf{a}_m = \mathbf{c}_p$, $\mathbf{b}_m = -\mathbf{a}_p - 2\mathbf{b}_p$, $\mathbf{c}_m = \mathbf{a}_p$). A graphical presentation of the various cell settings described here is shown in Fig. 1(d). An additional intermediate phase of space-group symmetry $C2$ from 950–450 K was proposed by Rodehorst *et al.*[4] A recent temperature-dependent structural investigation searched for this intermediate phase but found no evidence for its existence.[5] The $P2_1$ room-temperature phase is metrically monoclinic and of single-**q** type in that it only gives rise to

additional $\mathbf{G} \pm \frac{1}{2}[010]_p^*$-type satellite reflections and not to all the three distinct types of $\mathbf{G} \pm \frac{1}{2}\langle 010\rangle_p^*$ satellite reflections.

By contrast with $BaAl_2O_4$, although the room-temperature structure of $SrAl_2O_4$ is polar and potentially ferroelectric, only pyroelectric properties have been reported for $SrAl_2O_4$ to date.[10] Instead, the focus has been on its ferroelastic properties.[4] Recent studies, however, have reported ferroelectric hysteresis loops in ceramic Eu-doped samples (SAO-E).[14] This strongly suggests that similar ferroelectric behavior is to be expected in the pure compound. Note that the polar axis in the case of $SrAl_2O_4$ is in the *xy* plane of the parent phase, while it would correspond to the *z* direction in the reported $P6_3$ phase for $BaAl_2O_4$. $SrAl_2O_4$ and $BaAl_2O_4$ thus appear to have quite different room-temperature ferroic properties despite having an isomorphous $P6_322$ parent phase.

The recent electron microscopy results reported in Ref. 6 throw doubt on the long accepted room-temperature structure of $BaAl_2O_4$ and indicate that its behavior is rather more closely related to that of $SrAl_2O_4$ than had previously been considered. In addition, the phase diagram of the $(Ba_{1-x}Sr_x)Al_2O_4$ solid solution between these two end-member compounds is rather complex with coexistence of different phases over temperature intervals of hundreds of degrees.[3,4] These results have moved us to make a comparative investigation of both end-member compounds.

The *ab initio* calculations presented below include a quantitative characterization of the intriguing bilinear coupling between ferroelectric and ferroelastic properties in $SrAl_2O_4$, which allow the switching of the spontaneous polarization by means of a stress, and conversely, a switch of the spontaneous strain through an electric field. It is suggested that this strong and peculiar discontinuous piezoelectric response is most probably closely related with the strong electroluminiscent and elasticoluminiscent properties observed in Eu-doped $SrAl_2O_4$.[13,14]

II. TECHNICAL DETAILS OF THE *AB INITIO* CALCULATIONS

The linearized augmented plane wave+local orbitals code WIEN2K (Ref. 20) has been used. Exchange and correlation were treated within the generalized gradient approximation (GGA) by using the Perdew-Burke-Ernzerhof (PBE) parameterization.[21] The atomic sphere radii R_{mt} were chosen as 2.42, 1.37, and 1.37 bohr for Sr, Al, and O, respectively, in the case of $SrAl_2O_4$ and 2.50, 1.40, and 1.40 bohr for Ba, Al, and O, respectively, in the case of $BaAl_2O_4$. The parameter $R_{mt}K_{max}$ determining the plane-wave basis set was varied between 5.5 and 8 depending on the case and the accuracy required. Depending on the size of the unit cell or supercell used, the *k* mesh was varied to assess convergence, but typically $3\times2\times4$ shifted Monkhorst-Pack meshes were used for the orthorhombic or monoclinic structures and $2\times2\times2$ for the hexagonal configurations with the doubled basal plane cells. If nothing is said to the contrary, calculations were done using the experimental unit-cell parameters or their averaged symmetrized values when considering virtual structures with specific distortion modes. Internal structure relaxations searching for configurations of minimum energy were also carried out in general with unit cells fixed to the experimental values.

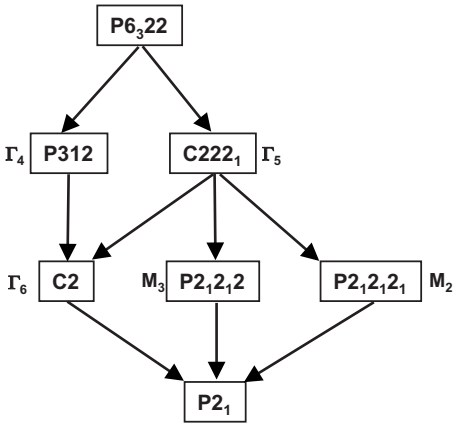

FIG. 2. The chain of maximal subgroups relating the symmetries of the HT and RT phases of $SrAl_2O_4$. For each space group, if a distortion mode yielding this symmetry is possible, the irreducible representation (irrep) of the HT $P6_322$ space group associated with this mode is indicated. The nomenclature of the irreps is that used by ISOTROPY (Ref. 23).

III. STRUCTURAL INSTABILITIES IN $SrAl_2O_4$

The hexagonal HT $P6_322$ parent structure of both $SrAl_2O_4$ and $BaAl_2O_4$ ($a_p \sim 5.167/5.224$, $c_p \sim 8.459/8.793$ Å) is defined by the following atomic positions within the asymmetric unit: Sr/Ba at $2b$ $[0\ 0\ \frac{1}{4}]$, Al at $4f$ $[\frac{1}{3}, \frac{2}{3}, 0.054/0.058]$, O1 at $2c$ $[\frac{1}{3}, \frac{2}{3}, \frac{1}{4}]$, and O2 at $6g$ $[0.63/0.65, 0, 0]$. The $P2_1$ structure of the RT phase of $SrAl_2O_4$, as given in Ref. 22, can be related to this aristotype structure through the cell transformation $\mathbf{a}_m=\mathbf{c}_p$, $\mathbf{b}_m=-\mathbf{a}_p-2\mathbf{b}_p$, and $\mathbf{c}_m=\mathbf{a}_p$, and a shift of origin of $[\frac{3}{4}, 0, \frac{3}{4}]_p$. Figure 2 shows the lattice of maximal subgroups [along with the associated irreducible representations (irreps) of $P6_322$] relating the prototype hexagonal $P6_322$ and RT monoclinic $P2_1$ symmetries, as obtained via the tools of the Bilbao Crystallographic Server.[24,25] The three irreps with label Γ correspond to zone-center ($\mathbf{q}=\mathbf{0}$) modes while the two irreps with label M correspond to zone-edge M point ($\mathbf{q}=[0,\frac{1}{2},0]_p^*$) modes. As pointed out by Rodehorst *et al.*,[4] there is no single irrep which, on its own, can explain the entire symmetry break from the parent $P6_322$ phase to the observed RT $P2_1$ phase. At least two distortion modes transforming according to two different irreps are necessary for explaining the symmetry transformation from the parent phase. The existence of an intermediate phase of space group $P6_3$ ($\sqrt{3}a_p\times\sqrt{3}a_p\times c_p$) does not change this basic fact. Note that the symmetry of this intermediate phase is not a supergroup of the $P2_1$ structure of the RT phase, contrary to a comment by Avdeev *et al.*[5]

With the aid of the program AMPLIMODES,[26] the reported $P2_1$ RT phase of $SrAl_2O_4$ (Ref. 22) has been decomposed into a $P6_322$ symmetrized reference structure plus the contributions of the various allowed symmetry-breaking distor-

TABLE I. Mode decomposition of the distortion relating the experimental $P2_1$ structure of the RT phase of $SrAl_2O_4$ (Ref. 22) with a symmetrized $P6_322$ configuration. Polarization vectors of each mode have been normalized within a unit cell of the RT phase. The second row indicates the dimension of the corresponding subspace. Results are compared with those obtained for the *ab initio* calculated structure relaxed under $P2_1$ symmetry. The second column for each mode indicates the scalar product of their polarization vectors with the one of the experimental structure. (Note: the polar distortion mode Γ_6 has been calculated subtracting the global translation present in the reported experimental structure when compared with the $P6_322$ configuration.)

Irrep	M_2-1**q**		Γ_6		M_3-1**q**		Γ_5		Γ_4	
Dim.	12		7		11		7		3	
	Amplitude	Product	Amplitude	Product	Amplitude	Product	Amplitude	Product	Amplitude	Product
Expt. Structure	1.70		1.39		0.57		0.32		0.02	
Ab initio this work (β=90°)	1.83	0.996	1.19	−0.9990	0.52	−0.989	0.23	0.93	0.07	−0.41
Ab initio this work (β=93.5°)	1.81	0.998	1.35	0.9997	0.57	0.997	0.24	0.96	0.03	0.63

tion modes. The hexagonal lattice parameters used were derived from those reported for the $P6_3(\sqrt{3}a_p)$ phase.[27] The resulting overall mode amplitudes (in Å), with the polarization vectors normalized to unity within a unit cell of the distorted RT structure, are listed in Table I. It can clearly be seen that there are two dominant (or primary) distortion modes with M_2 and Γ_6 symmetry. Note that the amplitude of the Γ_6 distortion mode, while large (at 1.39 Å), is nonetheless somewhat smaller than the amplitude of the M_2 distortion mode (at 1.70 Å). As indicated in Fig. 2, a condensed M_2 mode on its own would yield a structure with orthorhombic $P2_12_12_1$ [$a_p\times\sqrt{3}a_p\times c_p$, see Fig. 1(f)] symmetry, while a condensed Γ_6 mode on its own would give a structure with monoclinic $C121$ [$a_p\times\sqrt{3}a_p\times c_p$, see Fig. 1(e)] symmetry. The observed $P2_1$ configuration results when both distortion modes are present simultaneously, yielding a space group which is the intersection of the two mentioned above.

Both these dominant distortion modes correspond in essence to large-amplitude condensed rigid unit modes (RUMs) (see, e.g., Refs. 28–30) of the Al_2O_4 tetrahedral framework substructure correlated with smaller displacements of the Sr atoms stuffed on the hexagonal channels. Note that while infinitesimally small amplitude RUM modes do not involve an expansion in size of the constituent AlO_4 tetrahedra, the large amplitude of both the M_2 and Γ_6 RUM modes involved here [see Figs. 1(e) and 1(f)] are necessarily associated with a correlated expansion in size of the constituent AlO_4 tetrahedra. The M_2 mode [cf. Fig. 1(f) with Fig. 1(c)] involves coupled rotations and translations of the AlO_4 tetrahedra around the $[120]_p$ axis [out of the plane in Figs. 1(c) and 1(f)], while the Γ_6 mode [cf. Fig. 1(e) with Fig. 1(b)] largely involves coupled tetrahedral rotations and translations around the orthogonal $[100]_p$ axis [out of the plane in Figs. 1(b) and 1(e)]. Both modes separately are able to relax the initially unfavorable 180° Al-O-Al angles present in the $P6_322$ parent structure. In fact, when the program CRUSH (Ref. 28) is applied to determine the RUMs of the $P6_322$ tetrahedral Al_2O_4 framework substructure, the results indicate that the Γ_6 and M_2 modes frozen in the RT phase correspond to the end points of a whole branch of soft RUM modes along the $\langle 010\rangle_p^*$ directions, from the center of the Brillouin zone to the M points at its border. The irrep Γ_6, at $\mathbf{q}=\mathbf{0}$, is two dimensional. The observed Γ_6 distortion [see Fig. 1(e)] corresponds to a specific irrep direction which keeps $C121$ space-group symmetry. On the other hand, the M_2 mode is threefold degenerate with a three-dimensional order parameter associated with the three symmetry-related modulation wave vectors $\mathbf{q}_1=[0,\frac{1}{2},0]_p^*$, $\mathbf{q}_2=[-\frac{1}{2},0,0]_p^*$, and $\mathbf{q}_3=[\frac{1}{2},-\frac{1}{2},0]_p^*$. The $P2_12_12_1$ distortion in $SrAl_2O_4$ arises from the particular case where only one of these three M_2-type modulation waves is present in the overall distortion. Henceforth we label this mode the M_2-1**q** mode.

Apart from relaxing the 180° Al-O-Al angles present in the parent $P6_322$ structure, these two primary (Γ_6 and M_2-1**q**) modes also significantly improve the overall crystal chemistry of the system. Sr^{2+} ions at the center of the hexagonal channels of the undistorted HT phase, for example, are initially severely underbonded with an apparent valence or bond valence sum (BVS) (Refs. 31–33), of only 1.15. Likewise, the Al^{3+} ions in the undistorted HT structure are significantly overbonded with a BVS ~3.6. Clearly there is a need for large amplitude tetrahedral rotations and the associated expansion in size of the constituent AlO_4 tetrahedra in order to reduce the initial overbonding of the Al^{3+} ions while simultaneously improving the initial severe underbonding of the interstitial Sr^{2+} ions. A good way to measure this change in local crystal chemistry is via the square of the so-called global instability index, G_{ii}, defined as the root-mean-square deviation of the atomic bond valence sums of all atoms with respect to their nominal values (see Refs. 31 and 32).

Figure 3(a) shows the calculated variation in G_{ii}^2 as a function of mode amplitude, Q, for each of the two primary distortion modes as well as for the next highest amplitude M_3-1**q** mode. Note that the value of G_{ii}^2 systematically decreases from 0.21 in the HT structure to values of the order of 0.02 and 0.04 at the minima of the curves for the M_2-1**q** and the Γ_6 distortion modes, respectively. It is remarkable that the minima of these curves are so close to the mode amplitudes observed in the actual experimental structure (see Table I), although systematically larger for both modes. The combination of both modes in the experimental structure, plus the condensation of the additional induced secondary

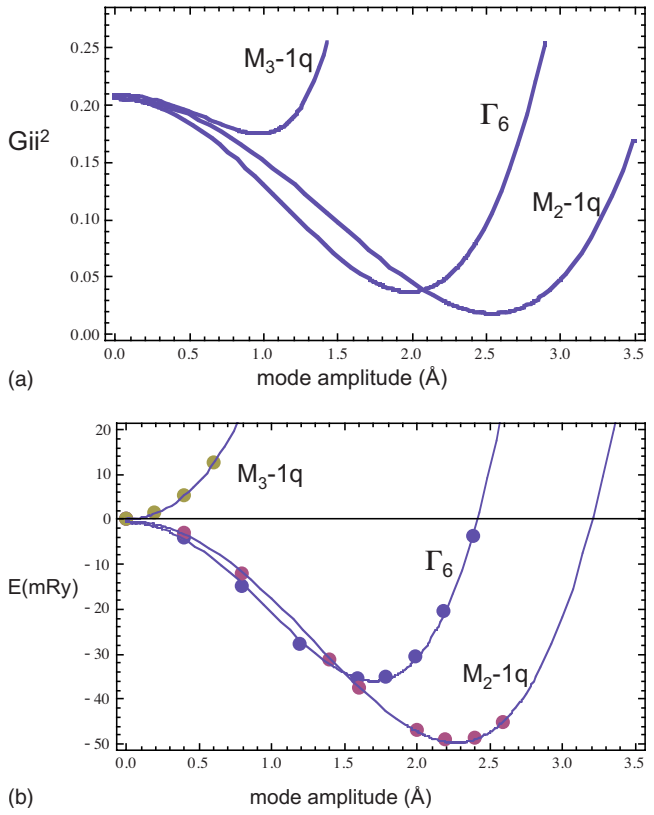

FIG. 3. (Color online) (a) Square of the global instability index, G_{ii}, calculated for $SrAl_2O_4$ as a function of the amplitude of the experimental distortion modes M_2-1q and Γ_6. (b) Calculated energy change in $SrAl_2O_4$ as a function of the amplitude of the experimental distortion modes M_2-1q and Γ_6. Energies are given in mRy per f.u. Mode amplitudes are given in Ångstroms using the $P2_1$ unit cell for the normalization of the mode polarization vectors.

modes, including the monoclinic lattice strain, further improves the value of G_{ii}^2 down to 0.018, with all ions having bond valence sum values close to the expected valence, except that of the Sr^{2+} ions which remain somewhat underbonded with bond valence sum values of the order of 1.6–1.7.

Using the program WIEN2K,[20] the energy variation in $SrAl_2O_4$ as a function of mode amplitude has also been calculated [see Fig. 3(b)]. The calculated energy of the structure decreased with respect to that of the parent $P6_322$ hexagonal configuration by ~50 mRy and by ~37 mRy per f.u. at the minima of the curves for the M_2-1**q** and the Γ_6 distortion modes, respectively. As for the G_{ii}^2 versus mode amplitude plot, the minima of these *ab initio* calculated curves are relatively close to the mode amplitudes observed in the actual experimental structure (see Table I), although again systematically larger.

It is remarkable that the overall shape, as well as the location of the minima, of the curves for the M_2-1**q** and Γ_6 distortion modes in the *ab initio* energy and G_{ii}^2 versus mode amplitude plots are so similar [cf. Figs. 3(a) and 3(b)]. Indeed, an approximate scale factor of about 0.25 Ry/squared valence unit relates the two types of curves. (In other compounds where a similar effect has been observed, the approximate scale factor was of the order of 0.5 Ry/squared valence unit.[34,35]) This represents a new example of the ability of G_{ii}^2 to closely mimic changes of the energy, particularly for low-energy or unstable primary distortion modes.[34,35] Note, however, that the agreement is not good for the M_3-1**q** mode. The energy variation with amplitude of this secondary mode, depicted in Fig. 3(b), clearly indicates that this is an energetically unfavorable or hard mode. Its presence in the actual experimental structure must be an induced effect, through coupling with the unstable M_2-1**q** and Γ_6 distortion modes.

According to both the energy and G_{ii}^2 calculations, the Γ_6 mode is more unstable in the sense that its negative curvature at $Q=0$ is larger. This curvature is expected to be thermally renormalized to positive values in the HT phase, but in general the more negative the curvature, the larger the temperature necessary to make the mode stable. The calculated energy landscape would be therefore consistent with a two-step transition sequence with the Γ_6 mode condensing at a higher temperature than the M_2-1**q** mode and resulting in an intermediate phase $C121$, as proposed by Rodehorst *et al.*[4] The M_2-1**q** mode, however, is ultimately more efficient in decreasing the overall energy as a result of its deeper energy minimum.

By comparison with the experimental mode amplitudes for the two primary distortion modes derived from the refined structure (see Table I), both sets of minima in Fig. 3 occur at systematically larger mode amplitudes. This suggests a lack of "co-operation" between the two primary distortion modes in minimizing the overall energy, i.e., there must be significant anharmonic coupling between the two primary distortion modes that penalizes their simultaneous presence leading to a reduction in individual mode amplitude. This was confirmed by calculation of a relaxed $P2_1$ structure [the cell parameters were kept fixed to the experimental values, except for the monoclinic angle whose small deviation (3.4°) from 90° was at first disregarded]. The calculated energy of this relaxed structure decreased with respect to that of the parent $P6_322$ hexagonal configuration by 59.8 mRy per f.u., about 10 mRy more than a distortion limited to the M_2-1**q** symmetry mode alone [see Fig. 3(b)].

The decomposition of this *ab initio* relaxed structure in terms of distortion modes is also shown in Table I. The agreement in mode amplitudes as well as polarization vectors between this relaxed structure and the equivalent values derived from experiment is excellent, particularly for the largest amplitude modes. Note that the calculated relaxed structure has opposite signs for three of the distortions. This corresponds to an equivalent twin-related structure (see Sn.4 below). Only the weakest distortion mode of Γ_4 symmetry is not well reproduced. The amplitude of this distortion mode, however, is so small that its normalized polarization vector is necessarily badly determined both in experimental and calculated structures. The excellent agreement between theory and experiment, both in mode amplitude as well as mode eigenvector, improved still further when the above structure optimization was repeated with a fixed monoclinic strain of 3.5°, corresponding to the absolute energy minimum (cf. Tables I and II and Fig. 4). Table II compares in more detail the polarization eigenvectors of the most important distortion modes for this latter calculation. The agreement in mode

TABLE II. Comparison of the polarization vectors of the three strongest distortion modes present in the $P2_1$ structure of $SrAl_2O_4$, extracted from the experimental structure (Ref. 22) and from the theoretical structure obtained *ab initio*. Each column shows the amplitude of one of the symmetry-adapted modes corresponding to a Wyckoff atomic orbit. For atomic positions with several orthogonal modes of the same symmetry, they are further labeled with a number in parenthesis.

Mode M_2-1**q**	Sr (1)	Sr (2)	Al (1)	Al (2)	Al (3)	O1 (1)	O1 (2)	O2 (1)	O2 (2)	O2 (3)	O2 (4)	O2 (5)
Expt. Structure	−0.15	0.10	−0.17	−0.22	−0.14	−0.11	−0.69	−0.53	0.06	−0.14	0.05	−0.31
Ab initio this work (β=93.5°)	−0.14	0.07	−0.15	−0.22	−0.13	−0.10	−0.69	−0.54	0.05	−0.11	0.02	−0.31

Mode Γ_6	Sr	Al (1)	Al (2)	O1	O2 (1)	O2 (2)	O2 (3)
Expt. Structure	0.09	−0.002	−0.02	−0.65	0.69	0.22	0.23
Ab initio this work (β=93.5°)	0.10	−0.01	−0.01	−0.64	0.70	0.22	0.22

Mode M_3-1**q**	Sr (1)	Sr (2)	Al (1)	Al (2)	Al (3)	O1 (1)	O1 (2)	O2 (1)	O2 (2)	O2 (3)	O2 (4)
Expt. Structure	0.58	−0.43	0.00	0.13	0.18	0.25	0.05	−0.48	0.33	0.11	0.12
Ab initio this work (β=93.5°)	0.61	−0.44	−0.01	0.14	0.13	0.28	0.02	−0.46	0.31	0.10	0.11

amplitude as well as mode eigenvector for the primary M_2-1**q** and Γ_6 distortion modes is nearly perfect, with any deviations practically within experimental error. The deviations, although larger, are also quite small even in the case of the secondary M_3-1**q** mode.

IV. FERROIC PROPERTIES OF $SrAl_2O_4$

According to the above analysis, the $P2_1$ RT phase of $SrAl_2O_4$ is the result of the freezing in of two quite distinct intrinsic structural instabilities: one at the zone center (Γ_6, **q**=**0**) and the other at the Brillouin-zone border of the HT hexagonal phase (M_2, $\mathbf{q}=\frac{1}{2}\mathbf{b}_p^*$). Ferroic properties can only be associated with the former Γ_6, **q**=**0** mode. This unstable mode is in fact intrinsically polar and potentially ferroelectric, yielding a macroscopic spontaneous polarization along the $[1,2,0]_p$ direction. A calculation using the nominal atomic valences and the experimental polar distortion yields an estimation for the resulting macroscopic spontaneous polarization P_s of 5.7 $\mu C/cm^2$. While not as large as in some perovskite ferroelectrics (see, e.g., Ref. 33), this value is nonetheless quite comparable to polarizations observed in other well-known ferroelectrics such as, e.g., triglycine sulphate (TGS) or potassium dihydrogen phosphate (KDP) (KH_2PO_4).[36]

The clear presence of a frozen polar mode in the RT phase of $SrAl_2O_4$, in conjunction with its energy landscape around the HT configuration [see, e.g., Fig. 3(b)], indicates that the system has a bistable configuration with respect to its spontaneous polarization, with potential ferroelectric properties if the system can be switched between these two configurations. Thus, contrary to what was stated by Zhurov *et al.*,[10] $SrAl_2O_4$ can be considered a ferroelectric of *proper* type, as the frozen polar distortion is not an induced effect but rather originates in an intrinsic instability.

Furthermore, the symmetry of the Γ_6 mode is in fact also the symmetry of the quite significant spontaneous monoclinic shear strain (β=93.4°) of the experimental RT structure, the system thus having ferroelastic properties.[4] A *proper* ferroelastic mechanism for this shear distortion can however be ruled out on the basis of energy calculations [see Fig. 4(a), top]. Rather, it is the intrinsic instability of the Γ_6 optical mode that induces the monoclinic shear strain [see Fig. 4(a), bottom] as a result of the allowed bilinear coupling between the unstable polar mode and the strain [see Eqs. (1) and (2) below]. In other words, a hypothetical clamped sample forced to maintain the orthogonality of the lattice axes would still exhibit the symmetry break to a monoclinic configuration through the condensation of the unstable polar Γ_6 mode. Figure 4(a) shows calculated energy curves as a function of the $P2_1$ monoclinic angle β, both not allowing (top) and allowing (bottom) the atomic positions to relax with respect to the HT hexagonal configuration. One can see that the HT structure has no pure elastic instability, the hexagonal configuration being the one of lowest energy with respect to a pure monoclinic strain of the lattice. However, the overall energy minimum decreases by a further 4.5 mRy per f.u. and is attained for $\beta \sim 93.5°$ (or equivalently 86.5°) when the atomic positions are allowed to relax, in very good agreement with the experimentally observed value of 3.4°.[22]

Figure 4(b) shows the calculated variation in the amplitudes of the primary distortion modes (M_2-1**q** and Γ_6) as a function of β when the atomic positions are relaxed. Note that the bilinear coupling between the monoclinic strain and the Γ_6 polar distortion mode means that a switch in sign of the monoclinic shear strain produces a corresponding switch in sign of the amplitude of the polar Γ_6 distortion mode (and therefore of the associated spontaneous polarization), while the amplitude of the M_2-1**q** mode remains essentially unchanged. Apart from this coupled ferroelectric/ferroelastic switching property, note the relatively strong linear dependence of the polar Γ_6 mode amplitude, $Q(\Gamma_6)$, upon the magnitude of the monoclinic shear strain, e.g., $Q(\Gamma_6)$ increases ~15% when β increases from 90° to the equilibrium angle 93.5°. The amplitude of the M_2-1**q** distortion mode by contrast hardly changes over the same range of β.

While the amplitudes of the two distortion modes behave very differently when the monoclinic strain is applied, their

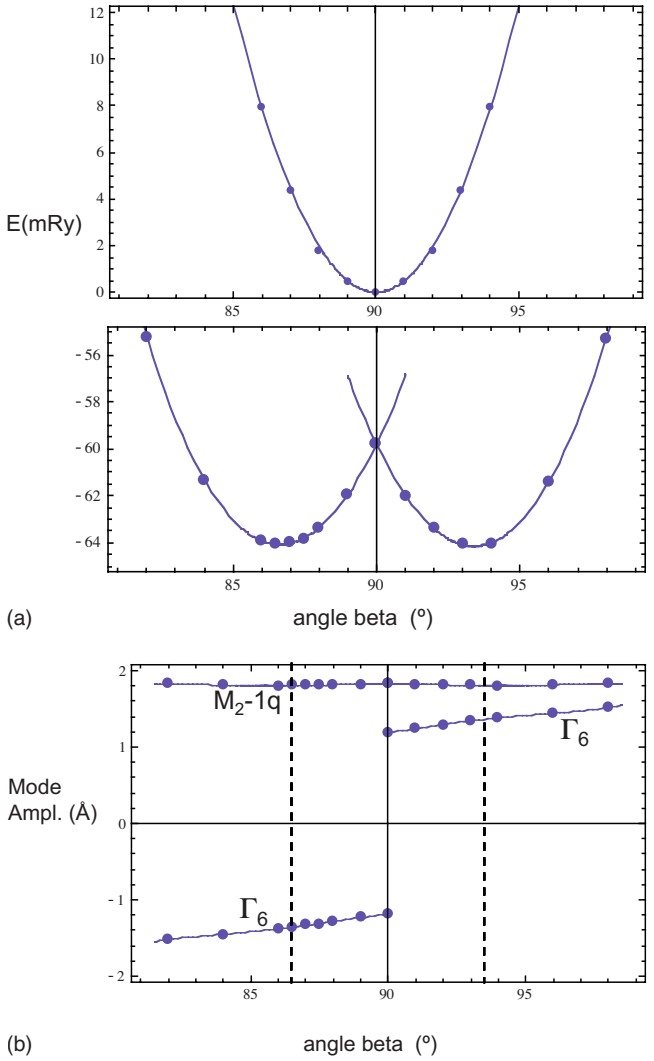

FIG. 4. (Color online) (a) Calculated energy variation (per f.u.) in $SrAl_2O_4$ constrained to the $P2_1$ space group as a function of the monoclinic angle β. Above: with atomic positions fixed to their values in the $P6_322$ configuration; below: with the atomic positions relaxed so that the total energy is minimized. (b) Amplitudes of the main distortion modes M_2-1q and Γ_6 for the relaxed configuration, as a function of the angle β. The dashed lines indicate the values corresponding to equilibrium.

polarization vectors only depend very weakly on the shear strain. The scalar product of their values for $\beta=90°$ and $\beta=93.5°$ deviate from unity less than 0.03. These results represent a clear illustration of how the modes of different symmetry which are frozen in a distorted crystalline structure behave as virtually "quasirigid" relative atomic displacements, having in general different responses to external perturbations.

From these considerations and the *ab initio* calculations discussed above, a definite picture of the ferroic properties of $SrAl_2O_4$ can be established. RT $SrAl_2O_4$ can be considered to be a proper ferroelectric as well as a pseudoproper ferroelastic. Twelve distinct domain types can be expected according to the index (12) of the subgroup $P2_1$ with respect to the parent space group $P6_322$.[37] First, there are three equivalent orientations [see Fig. 1(c)] of the monoclinic unit cell with respect to the hexagonal HT lattice, corresponding to the choice of one of the three modulation wave vectors associated with the M irreps. Second, for each of these three equivalent orientations, there are two possible distinct signs for the mode amplitudes of each of the two primary distortion modes, yielding four different equivalent configurations. These four distinct variants for a fixed orientation of the monoclinic unit cell will also include the presence of secondary modes, but their signs will be strictly correlated with those of the primary modes according to their respective coupling with them. The coupling terms of lowest order allowed by symmetry for the different secondary modes are

$$\begin{aligned} &Q_{\mathrm{M3\text{-}1q}}: \quad Q_{\mathrm{M3\text{-}1q}}Q_{\mathrm{M2\text{-}1q}}Q_{\Gamma 6}, \\ &Q_{\Gamma 5}: \quad Q_{\Gamma 5}(Q_{\mathrm{M2\text{-}1q}})^2, \quad Q_{\Gamma 5}(Q_{\Gamma 6})^2, \\ &Q_{\Gamma 4}: \quad Q_{\Gamma 4}(Q_{\Gamma 6})^3, \\ &\varepsilon_m: \quad \varepsilon_m Q_{\Gamma 6}. \end{aligned} \tag{1}$$

Considering in the lowest approximation the harmonic terms for each of these secondary modes plus these coupling terms, the induced secondary amplitudes would satisfy the following proportionality laws with respect to the primary modes:[38]

$$\begin{aligned} &Q^o_{\mathrm{M3\text{-}1q}} \sim Q^o_{\mathrm{M2\text{-}1q}}Q^o_{\Gamma 6}, \\ &Q^o_{\Gamma 5} \sim a(Q^o_{\mathrm{M2\text{-}1q}})^2 + b(Q^o_{\Gamma 6})^2, \\ &Q^o_{\Gamma 4} \sim (Q^o_{\Gamma 6})^3, \\ &\varepsilon^o_m \sim Q^o_{\Gamma 6}. \end{aligned} \tag{2}$$

The superscript ^{o} stresses that the equations refer to equilibrium values. These laws show the required changes in sign of the induced secondary mode amplitudes when the signs of the amplitudes of the primary distortion modes are independently switched. These sign correlations are forced by symmetry and are independent of the approximations included in Eq. (2). Hence the four variants or domains for a fixed orientation, described in terms of the equilibrium mode amplitudes of the primary and secondary modes, as well as the monoclinic shear strain ε^o_m of the lattice, are given by the following:

variant 1:

$$(Q^o_{\mathrm{M2\text{-}1q}},\ Q^o_{\Gamma 6},\ Q^o_{\mathrm{M3\text{-}1q}},\ Q^o_{\Gamma 5},\ Q^o_{\Gamma 4},\ \varepsilon^o_m),$$

variant 2:

$$(Q^o_{\mathrm{M2\text{-}1q}},\ -Q^o_{\Gamma 6},\ -Q^o_{\mathrm{M3\text{-}1q}},\ Q^o_{\Gamma 5},-Q^o_{\Gamma 4},\ -\varepsilon^o_m), \tag{3}$$

variant 3:

$$(-Q^o_{\mathrm{M2\text{-}1q}},\ Q^o_{\Gamma 6},\ -Q^o_{\mathrm{M3\text{-}1q}},\ Q^o_{\Gamma 5},\ Q^o_{\Gamma 4},\ \varepsilon^o_m),$$

and variant 4:

$$(-Q^o_{\mathrm{M2\text{-}1q}},\ -Q^o_{\Gamma 6},\ Q^o_{\mathrm{M3\text{-}1q}},\ Q^o_{\Gamma 5},\ -Q^o_{\Gamma 4},\ -\varepsilon^o_m).$$

Note that variants 2 and 4 have opposite electric polarization to variants 1 and 3, as the sign of $Q^o_{\Gamma 6}$ has been reversed, and

this switch of the spontaneous polarization requires correlated changes in sign of some secondary modes as well as of the monoclinic shear strain.

The pseudoproper ferroelastic character of the RT phase is given by the linear correlation of the equilibrium strain with the spontaneous polarization [see Eq. (2)], and implies that the latter can, in principle, be switched mechanically through the switch of the monoclinic shear strain by means of an adequate stress, as shown in the *ab initio* calculations discussed above. Conversely, the switching of the polarization through an electric field would also imply a switch of the shear strain. A strong shear elastoelectric effect is thus to be expected. This is especially relevant in light of the fact that $SrAl_2O_4$:Eu has recently been reported to exhibit electroluminescent emission proportional to both applied stress and applied electric field.[13–16] The above results suggest that the electric field and mechanical stress-induced luminescent properties of $SrAl_2O_4$:Eu are closely linked to the elastoelectric coupling described above, as a result of the proper ferroelectric and pseudoproper ferroelastic character of the system.

While $SrAl_2O_4$:Eu has recently been shown to be indeed ferroelectric,[14] only pyroelectric properties have previously been reported for pure $SrAl_2O_4$.[10] As mentioned above, while the ferroelectric properties of BaA_2O_4 have been studied and are known in the literature, the ferroelectric character of pure $SrAl_2O_4$ has been, in general, overlooked. In fact, most recent studies have focused on its ferroelastic properties alone.[4] The reasons for this situation are unclear. As discussed above, the expected magnitude of the spontaneous polarization, while not large, is comparable to well-known ferroelectrics and certainly similar to that present in $BaAl_2O_4$. The bulk energy barrier between the equivalent energy wells associated with the polar distortion, however, may be too large for allowing switching properties. From the calculations discussed above, this energy barrier can be estimated as ~15 to 20 mRy per f.u. The additional energy barrier required to change the sign of the monoclinic shear strain, ~5 mRy per f.u. [see Fig. 4(a)] has been included in this estimate. Such a barrier is certainly significantly larger than equivalent values in traditional ferroelectrics, e.g., ~7 mRy in $BaTiO_3$ (Ref. 39) or ~1 mRy in $SrBi_2Ta_2O_9$.[40] Another factor which also may have hampered the experimental characterization of the ferroic properties of this compound is the strong elastoelectric effect discussed above. The polarization switch requires a simultaneous switch of the monoclinic shear strain, which is of the order of 3.5°. This means that an experimental setup clamping the sample with respect to this shear would be unable to produce the ferroelectric switching. In addition, the fact that domains with different polarization are also ferroelastic domains with opposite shears certainly will limit the mobility of domain walls in the switching process at the mesoscopic level.

V. STRUCTURAL INSTABILITIES IN $BaAl_2O_4$

$BaAl_2O_4$ has the same $P6_322$ high-temperature (HT) phase as $SrAl_2O_4$. Below ~450 K, a phase transition to a $P6_3$ ($a=2a_p$) structure (RT phase) with a doubled hexagonal lattice parameter a is reported to occur.[3,19] The subgroup tree relating this symmetry to that of the parent HT phase is shown in Fig. 5. In this case, there is a single active M_2 irrep responsible for the entire observed symmetry break, along with two induced secondary distortion modes with different irreps that yield intermediate symmetries $P6_3$ (a_p) and $P6_322$ ($2a_p$), respectively.

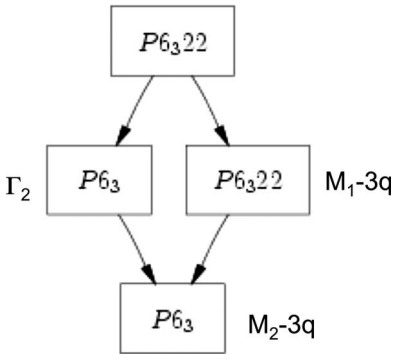

FIG. 5. Chain of maximal subgroups relating the reported symmetries of the HT and RT phases of $BaAl_2O_4$. For each space group, if a distortion mode yielding this symmetry is possible, the irreducible representation (irrep) of the HT $P6_322$ space group associated with this mode is indicated. The nomenclature of the irreps is that used by ISOTROPY (Ref. 23).

This active M_2 irrep is in fact the same one present in $SrAl_2O_4$ (the M_2-1**q** distortion mode). It is a three-dimensional irrep associated with three symmetry equivalent modulation waves with modulation wave vectors $\mathbf{q}_1$, $\mathbf{q}_2$, and $\mathbf{q}_3$, as given above. In the case of $P2_1$-type $SrAl_2O_4$, only one of these three modulation waves is present in the overall distortion. In the case of $P6_3$ ($a=2a_p$) $BaAl_2O_4$, however, all three such modulation waves must be simultaneously present and superposed coherently with the same amplitude.[9,23] The resultant $P6_3$ ($2a_p$) structure is polar, and would be an improper ferroelectric with an induced secondary polarization along the hexagonal axis. The symmetry of the induced polar mode corresponds to the irrep Γ_2 indicated in Fig. 6. The observation of a small spontaneous polarization observed in pyroelectric measurements has been explained along these lines.[8,9] Considerable doubt as to the validity of this $P6_3$ ($a=2a_p$) RT structure of $BaAl_2O_4$, however, has recently arisen as the result of poor fits to neutron-powder-diffraction data using this symmetry[6,41] combined with electron microscopy lattice imaging and subsequent fast Fourier transformation (FFT) data,[6] which shows that the $P6_3$ ($a=2a_p$) structure is not correct on the nanoscale.

In order to investigate the latter anomalies as well as the validity of the reported $P6_3$ ($a=2a_p$) RT structure of $BaAl_2O_4$ from the theoretical point of view, the experimental $P6_3$ ($2a_p$) structures reported in the literature (see Tables III and IV) have been decomposed in terms of symmetry modes, taking as reference the $P6_322$ structure reported by Perrota *et al.*[42] for the HT phase. The results are summarized in Table III. For comparison purposes, the mode decomposition of the $P6_3$ ($2a_p$) relaxed *ab initio* structure (calculated using WIEN2K) is also given. As the $P6_3$ ($a=2a_p$) structure given in Ref. 19 is the only single-crystal diffraction study up to now,

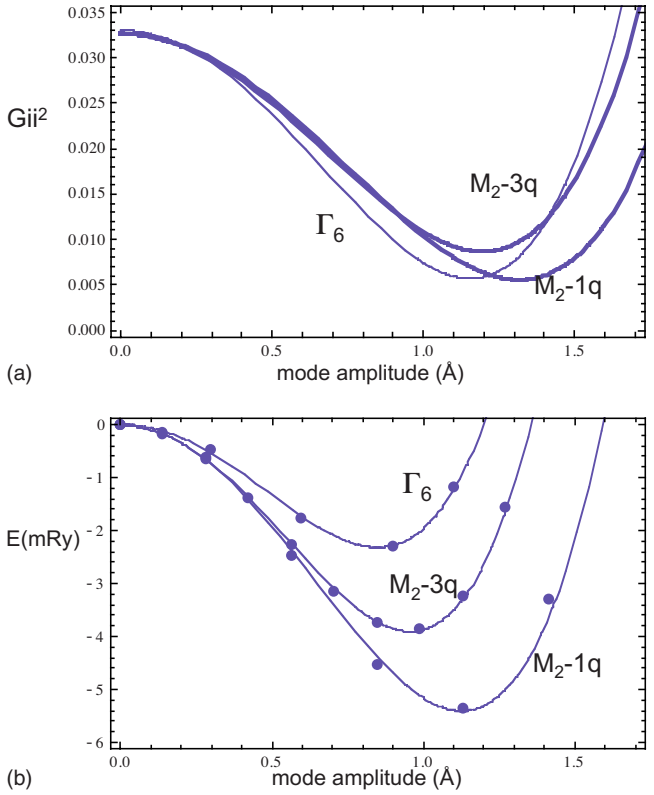

FIG. 6. (Color online) (a) Square of the global instability index G_{ii} for $BaAl_2O_4$ calculated as a function of the amplitude of the unstable modes M_2-3**q**, M_2-1**q**, and Γ_6. (b) Calculated energy change in $BaAl_2O_4$ as a function of the amplitude of the calculated unstable distortion modes M_2-3**q**, M_2-1**q**, and Γ_6. Energies are given in mRy per f.u. Mode amplitudes are given in Ångstroms using the $P2_12_12_1$ unit cell for the normalization of the mode polarization vectors.

the polarization vectors of the different distortion modes in Table III are quantitatively compared (by means of their scalar product) with those of this structure.[19] Clearly the polarization vector of the primary M_2-3**q** distortion mode is in very good agreement from one refinement to the next, including the *ab initio* calculation. The primary M_2-3**q** mode amplitude, however, varies quite strongly.

The most significant discrepancies from one refinement to the next, however, occur for the ferroelectric Γ_2 and M_1-3**q** secondary distortion modes. These not only have quite different amplitudes, but the agreement in polarization vector is also very poor. They differ not only with the polarization vectors corresponding to the structure in Ref. 19 but also among themselves. For instance, the scalar product of the normalized polarization vectors of the polar Γ_2 distortion mode present in the refinement models of Refs. 6 and 8 is only 0.32, indicating that the correlated atomic displacements involved are very different in the two models. Table IV lists in more detail the polarization vector of the ferroelectric Γ_2 distortion mode for the different published models, in terms of the amplitudes of the (normalized) symmetry-adapted modes associated with the different Wyckoff orbits. While in the model of Larsson *et al.*[6] the quite large polar displacements along z of the Al and Ba ions are in the same direction, in the model of Ref. 8 they have opposite directions. Similarly the important relative displacements of O1 ions with respect to O2 ions along z is more than three times larger in the model of Larsson *et al.*[6] than in the one of Huang *et al.*[8] Therefore, in the $P6_3$ $(2a_p)$ structural models proposed for this phase only the strong M_2-3**q** distortion mode seems robust.

The above discrepancies show some basic problems with the modeling of this phase using the reported $P6_3$ $(2a_p)$ symmetry. This is further supported by a comparison with the structure obtained from *ab initio* calculations. Again the secondary distortion modes deviate strongly from those proposed in the experimental studies. The most conspicuous difference concerns the ferroelectric Γ_2 distortion mode. This distortion mode is essentially negligible in the theoretical structure, while it has a significant amplitude in the experimental models (see Table III). This important discrepancy between the *ab initio* theoretical structural model and the experimental models contrasts with the excellent agreement of a similar comparison for $SrAl_2O_4$ (see Tables I and II).

TABLE III. Mode decomposition of the distortion relating the different experimental $P6_3$ structural models of the RT phase of $BaAl_2O_4$ with the configuration of its HT $P6_322$ phase. Polarization vectors of each mode have been normalized within a unit cell of the $P6_3$ phase. The second row indicates the dimension of each subspace. Results are compared with those obtained for the *ab initio* calculated structure relaxed under $P6_3$ symmetry. The second column for each mode lists the scalar product of the corresponding normalized polarization vector with the one proposed in the single-crystal diffraction study in Ref. 19. (Note: the polar distortion mode Γ_2 has been calculated subtracting the global translation present in the reported experimental structure when compared with the $P6_322$ configuration.)

Irrep	M_2-3**q**		M_1-3**q**		Γ_2	
Dim.	12		9		5	
	Amplitude	Product	Amplitude	Product	Amplitude	Product
Ref. 19	1.73		0.40		0.21	
Ref. 8	1.16	0.98	0.67	0.78	0.23	0.63
Ref. 42	1.32	0.98	0.62	0.45	0.16	0.90
Ref. 6	1.77	0.98	0.44	0.73	0.20	0.76
Ab initio (this work)	1.93	0.98	0.55	0.72	0.006	−0.42

TABLE IV. Comparison of the polarization vector of the Γ_2 polar mode present in the $P6_3$ $(2a_p)$ experimental models proposed for $BaAl_2O_4$. Each column shows the amplitude of one of the symmetry-adapted modes corresponding to a Wyckoff atomic orbit. For atomic positions with several (orthogonal) modes of the same symmetry, they are further labeled with a number in parenthesis.

Mode Γ_2	Ba	Al	O1	O2 (1)	O2 (2)
Ref. 19	−0.23	0.62	0.38	−0.59	−0.26
Ref. 8	−0.44	0.29	0.21	−0.10	−0.82
Ref. 41	−0.29	0.79	0.10	−0.54	0.03
Ref. 6	0.35	0.27	0.48	−0.70	−0.28

In light of the above problems, we have recently suggested[6] that the RT phase of $BaAl_2O_4$ may in fact be, at least locally, orthorhombic, or even monoclinic, instead of hexagonal. The relevant symmetries would then be those discussed above for $SrAl_2O_4$ and shown in Fig. 2. An orthorhombic configuration of $P2_12_12_1$ symmetry corresponds to the freezing of an M_2-1**q** distortion mode, while the space group would reduce further to monoclinic $P2_1$ if a polar Γ_6 distortion mode were also present. We have investigated this possibility by studying the stability of the HT configuration with respect to these types of distortions and comparing the results with those obtained by using modes of M_2-3**q** type. By means of symmetry-adapted frozen phonon calculations, the static normal displacive modes of Γ_6 and M_2 symmetry as well as their stiffness coefficients have been calculated. In each of the two subspaces there is indeed an unstable mode (i.e., with negative stiffness coefficient) (see Fig. 6). The polarization vectors of these modes are very similar to those present in $SrAl_2O_4$, and as stressed in Sn.3 for the Al_2O_4 framework, they correspond approximately to RUMs at the center and border of the Brillouin zone.

The calculated energy curves as a function of the amplitude of the unstable M_2 mode amplitude, for the alternative "directions" 1**q** and 3**q** and for the mode Γ_6, are shown in Fig. 6(b) and compared with the analogous curves obtained using G_{ii}^2 [see Fig. 6(a)]. By comparison with Fig. 3, it is clear that the instability in the case of $BaAl_2O_4$ is much weaker than for $SrAl_2O_4$. Both the depth of the energy wells and the improvement of the G_{ii}^2 value decrease one order of magnitude with respect to $SrAl_2O_4$. It is remarkable, that even in this case, with so small changes of energy and G_{ii}, the scaling between G_{ii}^2 and the energy behavior is still approximately maintained for the M_2-1**q** mode with a scale factor similar to the one observed in $SrAl_2O_4$. For the not so unstable Γ_6 mode, however, significant differences between the G_{ii}^2 and the energy behavior start to appear at such small scale. That the high-symmetry configuration is not so unstable for the Ba compound is clearly related to the larger size of the Ba cations inside the tridymite hexagonal channels. Compared with the Sr cations, the Ba cations fill more efficiently the channels (their bond valence sum is of the order of 1.6 compared with 1.15 for the Sr ions in $SrAl_2O_4$) so the tendency of these channels to collapse decreases, reducing the RUM instabilities of the tridymite framework.

The ferroelectric Γ_6 mode that is present in $SrAl_2O_4$ also lowers the overall energy in the case of $BaAl_2O_4$, but only weakly and relatively much less than does the M_2-1**q** distortion mode [cf. Fig. 6(b) with Fig. 3(b)]. Being such a weak instability, the Γ_6 mode is not expected to play such a relevant role as it does in the case of $SrAl_2O_4$. As suggested in Larsson *et al.*,[6] only the orthorhombic $P2_12_12_1$ configuration (corresponding to a condensed M_2-1**q** distortion mode alone) emerges as a possible alternative to the commonly accepted $P6_3$ $(2a_p)$ symmetry of the RT phase. A full relaxation of the *ab initio* $BaAl_2O_4$ structure assuming the $P2_1$ a symmetry of $SrAl_2O_4$ confirmed this assumption as the final optimized configuration yielded negligible amplitudes for all modes except those compatible with $P2_12_12_1$ symmetry (listed in Table V). This table compares the $P2_12_12_1$ structure proposed in Ref. 6 with the calculated relaxed structure, showing the basic agreement for the primary M_2-1**q** distortion mode

TABLE V. Mode decomposition of the distortion relating the calculated relaxed structure of $BaAl_2O_4$ under $P2_1$ symmetry. Only modes with non-negligible values are listed. These correspond to a distortion of higher symmetry $P2_12_12_1$. Polarization vectors of each mode have been normalized within a unit cell of the distorted phase. The second row indicates the dimension of each subspace. Results are compared with those obtained for the $P2_12_12_1$ model proposed in Ref. 6 but averaging the positions of the split atomic sites. The second column for each mode lists the scalar product of the corresponding normalized polarization vectors of the two models. In the fourth row, we list the amplitude corresponding to the energy minimum for the unstable M_2-1**q** distortion mode [see Fig. 6(b)], and the scalar product of its polarization vector with the one present in the relaxed structure.

Irrep	M_2-1**q**		Γ_5	
Dim.	12		7	
	Amplitude	Product	Amplitude	Product
Relax. Structure	1.22		0.19	
Expt.[a]	0.92	−0.95	0.21	0.47
Ab initio unstable mode	1.1	0.996		

[a]Reference 6.

Figure 6(b) shows that the M_2-1**q** mode yielding a $P2_12_12_1$ configuration is not only competitive with the M_2-3**q** distortion mode, but, in fact, corresponds to the absolute energy minimum for a M_2 distortion alone. This is corroborated by the behavior of G_{ii}^2 shown in Fig. 6(a). To be noted is the equal curvature of both energy curves around the zero-amplitude maximum, consistent with the degeneracy of the corresponding M_2 modes. Accordingly, if the contributions of induced secondary distortion modes were neglected, the equilibrium configuration of $BaAl_2O_4$ would correspond to orthorhombic $P2_12_12_1$ symmetry, with an energy decrease of about 1.5 mRy per f.u. with respect to the hexagonal M_2-3**q** option. However, in order to compare the relative stability of the $P6_3$ $(2a_p)$ and $P2_12_12_1$ options, one has to include the contribution of the secondary distortion modes triggered in each case, and therefore compare the calculated energies of fully relaxed structures constrained in both symmetries. From such a calculation, the secondary induced distortion modes associated with the hexagonal configuration

(the M_1-3**q** and Γ_2 modes) are somewhat more efficient in further decreasing the overall energy than those associated with the orthorhombic configuration so that the calculated equilibrium $P6_3$ ($2a_p$) structure results to be slightly more stable than the $P2_12_12_1$ configuration. The overall energy difference between the two alternative configurations, however, is very small, i.e., less than 1 mRy per f.u. It might well be that this very small energy difference could be obliterated either by thermal effects or local mesoscopic constraints in real samples, thereby explaining the electron microscope observations of the local stabilization of nonhexagonal configurations.[6]

It is interesting to compare this scenario with the one in $SrAl_2O_4$. If the energy variation with amplitude of the experimental M_2-1**q** distortion mode is compared in $SrAl_2O_4$ with the one corresponding to an hypothetical M_2-3**q** distortion mode calculated adding three symmetry-related M_2-1**q** distortions, the result is analogous to that obtained for $BaAl_2O_4$ [see Fig. 6(b)] but on a much larger scale. The energy minimum of the M_2-1**q** distortion is more than 15 mRy per f.u. deeper than the hexagonal one, i.e., one order of magnitude larger than in $BaAl_2O_4$. Nevertheless, the additional relaxation with respect to the secondary modes again makes the hexagonal configuration highly competitive with the monoclinic one. In fact, only the additional energy decrease of about 4.2 mRy per f.u. attained in the monoclinic configuration through the spontaneous shear strain (see Fig. 4) makes the monoclinic configuration more stable than the hexagonal $P6_3$ ($2a_p$) configuration. The energy difference in favor of the monoclinic structure in $SrAl_2O_4$ is in fact less than 3 mRy per f.u.

It is important to note that the polar Γ_6 instability of $SrAl_2O_4$, although weaker, is also *latent* in $BaAl_2O_4$ [see Fig. 6(b)]. A distortion of this symmetry is not present in the Ba compound because its instability is too weak to prevail over the energy cost of its anharmonic coupling with the dominant antiferrodistortive M_2 distortion. This situation can change if a external perturbation favors somehow the latent polar instability. One can therefore speculate that a sufficiently large applied electric field along the $[120]_p$ direction, or a shear stress on the perpendicular plane, could stabilize in $BaAl_2O_4$ a $P2_1$ phase analogous to the one observed in $SrAl_2O_4$, thus giving place to conspicuous dielectric and piezoelectric responses at some particular values of the applied field.

VI. CONCLUSIONS

By means of *ab initio* energy calculations, the similarities and differences between the structures and associated ferroic properties of $SrAl_2O_4$ and $BaAl_2O_4$ have been investigated. We have applied a systematic decomposition of experimental and calculated structures into symmetry-adapted distortion modes. This allows us to separate and identify the collective degrees of freedom that play an active role in the stabilization of the low-temperature phases, and to compare them with results from frozen phonon mode calculations. Furthermore, a description in terms of symmetry-adapted modes allows a quantitative study of the very different response that these distortion modes may have to external perturbation, as shown here by the mode analysis of the structural variation in $SrAl_2O_4$ as a function of its shear monoclinic strain. A comparison of different refined structural models in terms of distortion modes also makes plain the different degrees of accuracy with which the different symmetry components present in the structural distortions have been determined. Induced secondary modes have in general weaker amplitudes and are thus more poorly determined.

The strongest primary distortion mode in the two compounds corresponds to an antiferrodistortive RUM triply-degenerate mode M_2 of the Al_2O_4 tetrahedral framework combined with small displacements of the Sr and Ba cations within the hexagonal tunnels. Two alternative M_2 distortions with one or three distortion waves (M_2-1**q** and M_2-3**q**) are very competitive in both compounds. In $BaAl_2O_4$ the hexagonal M_2-3**q** configuration slightly prevails due to the contribution of additional induced secondary distortion modes. The balance could be reversed in real samples by local defects and constraints, thus explaining the orthorhombic local signatures recently observed via electron microscopy.[6]

In the case of $SrAl_2O_4$, the above delicate balance between the two alternative configurations changes in the other sense due to an additional polar instability at the Brillouin-zone center, which is present in both compounds, but much stronger in $SrAl_2O_4$. Again here, an induced effect, namely, the small monoclinic strain associated with the monoclinic equilibrium configuration, plays a fundamental role to make the M_2-1**q** configuration prevail.

$SrAl_2O_4$ has been shown to have the features of a proper ferroelectric and a pseudoproper ferroelastic, with an uncommon linear coupling between the spontaneous electric polarization and the spontaneous monoclinic shear strain, which may lead to peculiar elastoelectric effects. The bulk energy barrier for this process is however larger than in standard ferroelectrics. $BaAl_2O_4$, on the other hand, in its hexagonal configuration is an improper ferroelectric. The electric polarization is produced by an induced secondary distortion mode, which has no intrinsic instability. In fact, calculations predict a much smaller amplitude for this secondary polar distortion mode than those obtained from experimental structural studies. This is in qualitative agreement with the fact that the electric polarization in this compound is reported to have a conspicuous behavior, decreasing as temperature is lowered. The reason for an apparent thermal enhancement of this secondary polar distortion mode is not clear, but certainly it is not the ferrielectric mechanism proposed in Ref. 8 since this would require that the polar mode(s) would be intrinsically thermally unstable, and this can be ruled out by the above energy calculations.

Finally, all through this work the *ab initio* ground-state energy calculations reported have been compared with calculations based on the bond valence method.[31] More specifically, energy variations have been compared with corresponding changes in the so-called global instability index,[32] which measures the chemical stress in a structure. The striking similarity in the behavior of both quantities for unstable distortion modes of the parent high-symmetry configuration, which has also been reported in other systems,[34,35] is again observed in these two ferroic compounds.

ACKNOWLEDGMENTS

Financial support from the Spanish Ministry of Science and Technology (Project No. MAT2005-05216), the Basque Government (Project No. IT-282-07), and the Australian Research Council in the form of ARC Discovery Grants (R.L.W. and Y.L.) are gratefully acknowledged. Part of the computer time was provided by the SGI/IZO-SGIker at the UPV/EHU (supported by the Spanish Ministry of Education and Science and the European Social Fund). J.M.P.-M. acknowledges support of the Research School of Chemistry (ANU) for a working visit at the ANU.

[1] C. M. B. Henderson and D. Taylor, Mineral. Mag. **45**, 111 (1982).
[2] D. Taylor, M. J. Dempsey, and C. M. B. Henderson, Bull. Mineral. **108**, 643 (1985).
[3] A. M. Abakumov, O. I. Lebedev, L. Nistor, G. Van Tendeloo, and S. Amelinckx, Phase Transit. **71**, 143 (2000).
[4] U. Rodehorst, M. A. Carpenter, S. Marion, and M. B. Henderson, Mineral. Mag. **67**, 989 (2003).
[5] M. Avdeev, S. Yakovlev, A. A. Yaremchenko, and V. V. Kharton, J. Solid State Chem. **180**, 3535 (2007).
[6] A.-K. Larsson, R. L. Withers, J. M. Perez-Mato, J. D. Fitz Gerald, P. J. Saines, B. J. Kennedy, and Y. Liu, J. Solid State Chem. **181**, 1816 (2008).
[7] A. A. Bush and A. G. Laptev, Sov. Phys. Solid State **31**, 535 (1989).
[8] S.-Y. Huang, R. von der Muell, J. Ravez, J. P. Chaminade, P. Hagenmuller, and M. Couzi, J. Solid State Chem. **109**, 97 (1994).
[9] H. T. Stokes, C. Sadate, D. M. Hatch, L. L. Boyer, and M. J. Mehl, Phys. Rev. B **65**, 064105 (2002).
[10] V. V. Zhurov, A. A. Bush, S. A. Ivanov, S. Y. Stefanovich, and B. N. Romanov, Sov. Phys. Solid State **33**, 960 (1991).
[11] Y. Lin, Z. Zhang, Z. Tang, J. Zhang, Z. Zheng, and X. Lu, Mater. Chem. Phys. **70**, 156 (2001).
[12] H. Takasaki, S. Tanabe, and T. Hanada, J. Ceram. Soc. Jpn. **104**, 322 (1996).
[13] C. N. Xu, H. Yamada, X. Wang, and X. G. Zheng, Appl. Phys. Lett. **84**, 3040 (2004).
[14] Y. Liu and C. N. Xu, Appl. Phys. Lett. **84**, 5016 (2004).
[15] H. Yamada and C. N. Xu, J. Appl. Phys. **102**, 126103 (2007).
[16] H. Yamada, H. Kusaba, and C. N. Xu, Appl. Phys. Lett. **92**, 101909 (2008).
[17] W. Depmeier, in *Structures and Structure Determination*, edited by H. Karge and J. Weitkamp (Springer, New York, 1999), Vol. 2.
[18] K. Fukuda, T. Iwata, and T. Orito, J. Solid State Chem. **178**, 3662 (2005).
[19] V. W. Horkner and H. Muller-Buschbaum, Z. Anorg. Allg. Chem. **451**, 40 (1979).
[20] P. Blaha, K. Schwarz, G. Madsen, D. Kvasnicka, and J. Luitz, *WIEN2K, an Augmented Plane Wave+Local Orbitals Program for Calculating Crystal Properties* (Karl-Heinz Schwarz, Technische Universität Wien, Austria, 2001).
[21] J. P. Perdew, K. Burke, and M. Ernzerhof, Phys. Rev. Lett. **77**, 3865 (1996).
[22] A. R. Schulze and H. Mueller-Buschbaum, Z. Anorg. Allg. Chem. **475**, 205 (1981).
[23] H. T. Stokes, D. M. Hatch, and B. J. Campbell, ISOTROPY (stokes.byu.edu/isotropy.html) 2007.
[24] M. I. Aroyo, A. Kirov, C. Capillas, J. M. Perez-Mato, and H. Wondratscheck, Acta Crystallogr. A **62**, 115 (2006).
[25] M. I. Aroyo, J. M. Perez-Mato, C. Capillas, E. Kroumova, S. Ivantchev, G. Madariaga, A. Kirov, and H. Wondratscheck, Z. Kristallogr. **221**, 15 (2006).
[26] AMPLIMODES in the Bilbao Crystallographic Server (www.cryst.ehu.es).
[27] K. Fukuda and K. Fukushima, J. Solid State Chem. **178**, 2709 (2005).
[28] K. D. Hammonds, M. T. Dove, A. P. Giddy, and V. Heine, Am. Mineral. **79**, 1207 (1994).
[29] M. T. Dove, A. K. A. Pryde, V. Heine, and K. D. Hammonds, J. Phys.: Condens. Matter **19**, 275209 (2007).
[30] M. T. Dove, A. K. A. Pryde, and D. A. Keen, Min. Mag. (Lond.) **64**, 267 (2000).
[31] I. D. Brown, *The Chemical Bond in Inorganic Chemistry: The Bond Valence Method* (Oxford University Press, Oxford, 2002).
[32] A. Salinas-Sanchez, J. L. Garcia-Muñoz, J. Rodriguez-Carvajal, R. Saez-Puche, and J. L. Martinez, J. Solid State Chem. **100**, 201 (1992).
[33] R. L. Withers, J. G. Thompson, and A. D. Rae, J. Solid State Chem. **94**, 404 (1991).
[34] I. Etxebarria, J. M. Perez-Mato, A. García, P. Blaha, K. Schwarz, and J. Rodriguez-Carvajal, Phys. Rev. B **72**, 174108 (2005).
[35] J. M. Perez-Mato, P. Blaha, K. Schwarz, M. Aroyo, D. Orobengoa, I. Etxebarria, and A. García, Phys. Rev. B **77**, 184104 (2008).
[36] M. E. Lines and A. M. Glass, *Principles and Applications of Ferroelectrics and Related Materials* (Oxford University Press, Oxford, 1977).
[37] V. Janovec and J. Privratska, in *Domain Structures*, edited by A. Authier, International Tables for Crystallography Vol. D (Kluwer, Dordrecht, 2003), pp. 449–505.
[38] E. K. H. Salje, *Phase Transitions in Ferroelastic and Co-elastic Crystals* (Cambridge University Press, Cambridge, 1990).
[39] R. D. King-Smith and D. Vanderbilt, Phys. Rev. B **49**, 5828 (1994).
[40] J. M. Perez-Mato, M. Aroyo, A. García, P. Blaha, K. Schwarz, J. Schweifer, and K. Parlinski, Phys. Rev. B **70**, 214111 (2004).
[41] P. J. Saines, M. M. Elcombe, and B. J. Kennedy, J. Solid State Chem. **179**, 613 (2006).
[42] A. J. Perrotta and J. V. Smith, Bull. Soc. Fr. Mineral. Cristallogr. **91**, 85 (1968).